Journal of Alloys and Compounds 791 (2019) 1159–1166

Contents lists available at ScienceDirect

Journal of Alloys and Compounds

journal homepage: http://www.elsevier.com/locate/jalcom

Tunable electronic structure and structural transition of GaAs clusters at high pressure and temperature

Mustafa Kurban

Department of Electronics and Automation, Ahi Evran University, 40100 Kırşehir, Turkey

ARTICLE INFO

Article history:
Received 21 January 2019
Received in revised form
28 March 2019
Accepted 30 March 2019
Available online 2 April 2019

Keywords:
GaAs
Phase transitions
Electronic structure
Band engineering

ABSTRACT

In this study, the electronic structure and structural transition of the GaAs clusters with different compositions were examined by quantum chemical calculations for the first time. The GaAs clusters exhibit highly interesting structural and electronic properties as a function of composition, temperature, and pressure. The phase transitions were observed from the zinc blende structure ($P\bar{4}3m$) to the triclinic ($P\bar{1}$) and the tetragonal ($P\bar{4}$) structure where there are two and four intermediate phases, respectively. The As-rich clusters are generally more stable than that of the Ga-rich. The HOMO, LUMO and gap energies, Fermi levels, dipole moments and density of states were analyzed. The gap energy for the Ga_8As_{32} cluster was predicted as about 1.22 eV wide, i.e., about 0.29 eV smaller than the measured band gap of bulk $Ga_{0.5}As_{0.5}$ 1.51 eV at T = 0 K, while the gap energy for the $Ga_{32}As_8$ is found to be 0.15 eV. The Ga_8As_{32} and $Ga_{32}As_8$ clusters show semiconductor characters with high and low band energy at different pressures, while the $Ga_{32}As_8$ cluster shows metallic character under heat treatment. The trend of energy gap of the clusters is also compatible with available experimental findings.

1. Introduction

Gallium arsenide (GaAs), among III-V binary compound semiconductors, is the most important representative due to its use in the high-efficiency solar cell [1]. In this regard, GaAs has been subject of intensive research in both experimentally and theoretically to understand the structural, mechanical, thermal and electronic properties and demonstrate a highly efficient property of this material [2–8]. The properties of materials at nanolevel modify the traditional electronic structures. This gives rise to new opportunities for semiconductors and their applications in optoelectronic, photovoltaic and solar cell applications. For example, the optical properties of GaAs enhance at the nanoscale because of the change in the energy gap of GaAs [9]. Recently, the enhanced properties obtained from the changes in size and shape or optical and electrical control of GaAs quantum dots (QDs) have been shown in different studies [10,11].

GaAs crystallizes in the zinc blende phase (*ZB*) that undergoes pressure induced phase transformations. Most of the previous studies about the phase transformation of binary GaAs were related to the $Ga_{1-x}As_x$ (x = 0.5) except for ternary alloys of GaAs such as $Al_2Ga_5As_7$ [12] and $GaAs_{1-x}P_x$ [13]. Many studies have been performed on the $Ga_{0.5}As_{0.5}$ to examine phase transformation behavior based on the pressure or temperature. For example, the *ZB* structure of GaAs is transformed into an orthorhombic structure at almost 17 GPa [14,15]. By the experimental observations, GaAs transforms to GaAs-I (*ZB*) → GaAs-II (*Pmm*2) → GaAs-III (*Imm*2) →GaAs-IV (*P*6/*mmm*) at corresponding pressures 17, 24 and 60 GPa, respectively [16]. Furthermore, GaAs-II (*ZB*) structure was found as thermodynamically preferred orthorhombic structure over the rock salt structure with space group $Fm\bar{3}m$ by ab-initio calculations [17]. GaAs (*ZB*) the semiconducting phase at high pressure and temperatures transforms to the orthorhombic metallic phase with *Cmcm* symmetry [18], which is more stable than *Pmm*2 [19].

On the basis of the above mentioned, the structural properties and electronic structure of binary GaAs based on the composition at high pressures and temperatures have not been yet completed. Therefore, the primary scope of this work is to gain insights concerning phase transform behavior under heat treatment and at high hydrostatic pressure based on the composition in GaAs. In these regards, the structural mechanism properties such as the energy-volume relationships, intermediate states, enthalpy, segregation formation, radial distribution function, and the change of lattice parameters have been studied at high pressure. After that, the

E-mail addresses: mkurbanphys@gmail.com, mkurban@ahievran.edu.tr.

https://doi.org/10.1016/j.jallcom.2019.03.404
0925-8388/

electronic properties such as the HOMO, LUMO, Fermi and the gap energies and dipole moments under high pressure and temperature were analyzed and compared with experimental data in detail.

2. The method of calculations

The ab initio quantum chemistry calculations of the cubic GaAs (*ZB*) semiconducting phase were performed under pressure using the SIESTA [20] program. The Perdew-Burke-Ernzerhof (GGA-PBE) functional [21] was used with "double ζ (DZ) basis set". The cut off energy was chosen as 350 Ryd. The 8 × 8 × 8 Monkhorst-Pack (MP) mesh [22] were used in Brillouin region for all phases. Using the Conjugate Gradient technique, the pressure is increased by stages (10 GPa). 1.0 fs is used for each minimization step. Each simulation step was analyzed by the KPLOT [23] program and the RGS [24] algorithm, which provides data concerning the lattice parameters, space group and atomic positions in detail. The mechanism phase transformations were visualized by the CrystalMaker software. The DFTB + code [25] with the hyb-0-2 [26,27] set of Slater Koster parameters was used to examine the electronic properties.

3. Results and discussions

3.1. Structural analysis

The optimized geometries of the $Ga_{1-x}As_x$ (x = 0.20 and 0.80) clusters at 0 K and 0 GPa were indicated in Fig. 1. The Ga_8As_{32} and $Ga_{32}As_8$ unit cells were characterized by the zinc blende structure ($P\bar{4}3m$) and contain 40 atoms. The unit cell lattice constants at the equilibrium were predicted as a = 4.7917 Å for the Ga_8As_{32} and a = 5.0149 Å for the $Ga_{32}As_8$ cluster. The relaxed lattice parameters, bulk modulus, and corresponding pressure derivatives (at 0 GPa) of the Ga_8As_{32} and $Ga_{32}As_8$ clusters were given in Table 1. The obtained results were also compared with available experimental and theoretical $Ga_{0.5}As_{0.5}$ bulk results [13,28–30] (see Table 1). The variation of the volume based on the pressure was displayed in Fig. 2. The volume smoothly decreases after and before phase transformations occur, while the change in the volume was sharply observed from 30 GPa to 40 GPa and from 60 GPa to 70 GPa for the Ga_8As_{32} and $Ga_{32}As_8$ clusters, respectively. These results indicate that the pressure gives rise to a first order phase transition in the Ga_8As_{32} and $Ga_{32}As_8$ clusters, where the *ZB* structure converts into a triclinic (the space group $P\bar{1}$) structure at 40 GPa and tetragonal (the space group $P\bar{4}$) structure at 70 GPa for the Ga_8As_{32} and $Ga_{32}As_8$ clusters, respectively. Thus, the Ga_8As_{32} and $Ga_{32}As_8$ clusters depend highly on the composition. The As-rich cluster transforms earlier than that of the Ga-rich. In the literature, there is no information concerning composition dependence properties of GaAs at high pressure and temperature except for ternary GaAsX (Se, Al, P etc.) and binary $Ga_{05}As_{0.5}$ under high pressure which are mentioned in the section of introduction.

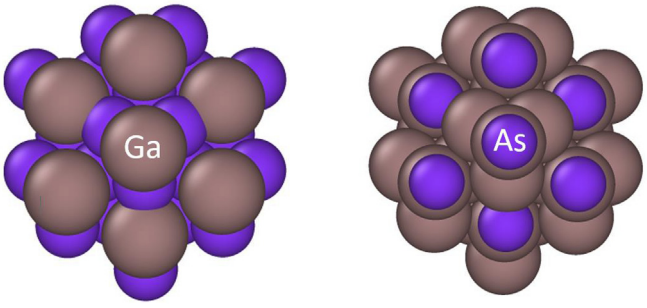

Fig. 1. The optimized geometries of the Ga_8As_{32} (left) and $Ga_{32}As_8$ (right) clusters (at 0 K and 0 GPa).

Table 1
The equilibrium lattice constants (a), bulk modulus (B_0) and their pressure derivatives (B_0') (at 0 K and 0 GPa).

Structure	a (Å)	B_0 (GPa)	B_0'
Ga_8As_{32}	4.791	73.86	4.17
$Ga_{32}As_8$	5.014	50.15	4.24
Bulk (Exp.)[a,b,c]	5.640	77.00	4.00
Bulk (Theory)[d]	5.603	73.46	4.84

[a] [28].
[b] [29].
[c] [29].
[d] [13].

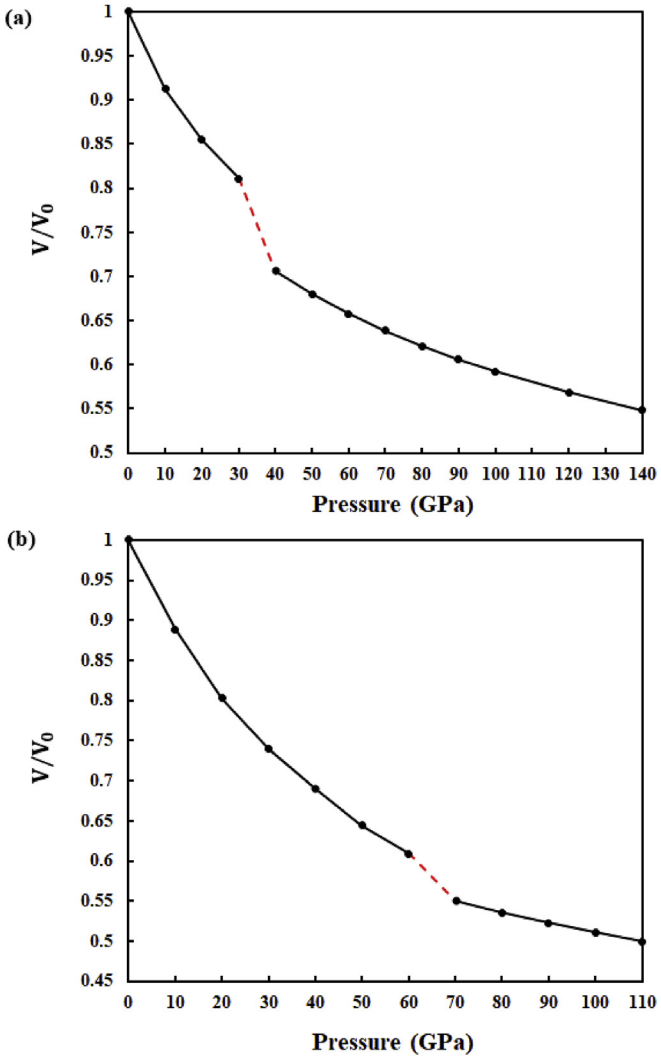

Fig. 2. The volume change of the simulation cell as function of pressure for (a) the Ga_8As_{32} and (b) $Ga_{32}As_8$ clusters.

The thermodynamic theorem cannot determine the energy of the transition barriers that separate possible two phases, thus the energy-volume relationships (see Fig. 3) was examined to find out the stability of the *ZB* and new structures triclinic and tetragonal obtained after phase transformations. Fig. 3 shows that the most stable phase is $P\bar{1}$ for the Ga_8As_{32} cluster and $P\bar{4}$ for and the $Ga_{32}As_8$ cluster.

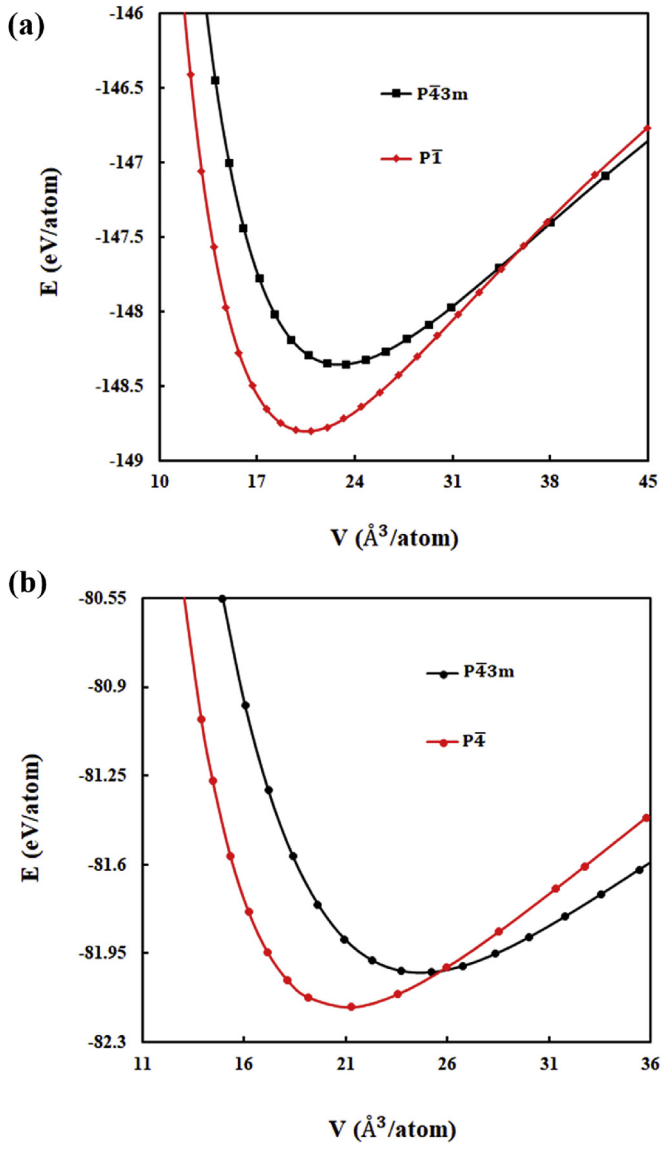

Fig. 3. The energy-volume curves of main structural phases for (a) the Ga_8As_{32} and (b) $Ga_{32}As_8$ clusters.

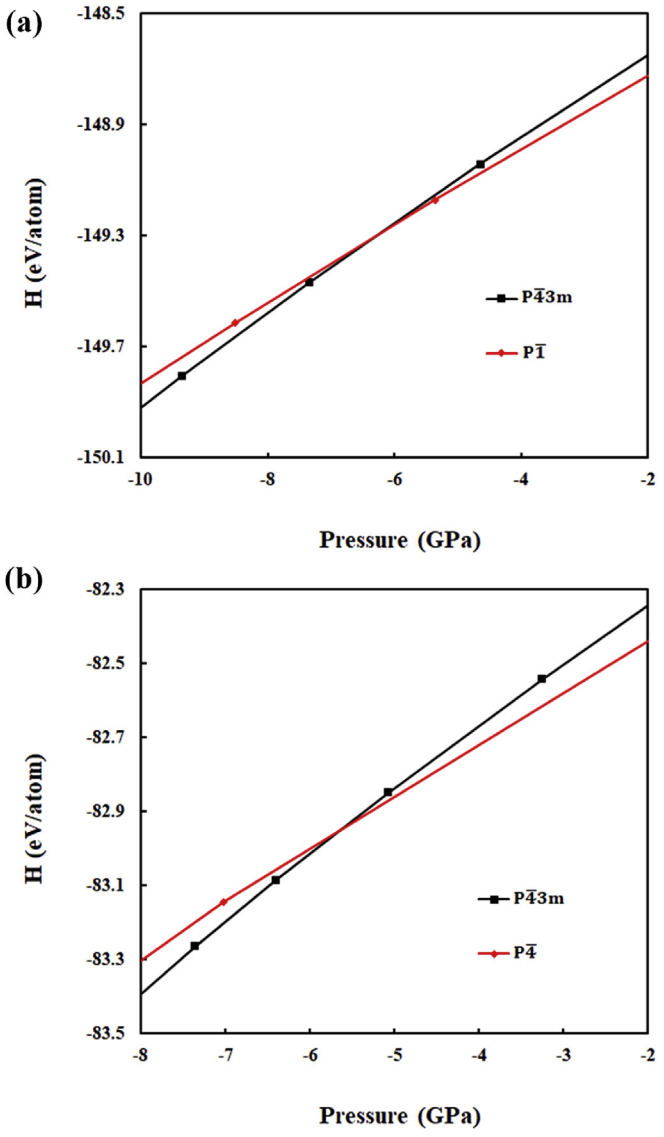

Fig. 4. The enthalpy curves of main structural phases for (a) the Ga_8As_{32} and (b) $Ga_{32}As_8$ clusters.

Based on the energy-volume data, the third-order Birch-Murnaghan equation of state [31,32] was used to calculate bulk modulus (B_0) and their pressure derivatives ($B_0^{'}$)

$$P = 1.5B_0\left[\left(\frac{V}{V_0}\right)^{-\frac{7}{3}} - \left(\frac{V}{V_0}\right)^{-\frac{5}{3}}\right]x\left\{1 + 0.75\left(B_0^{'} - 4\right)\left[\left(\frac{V}{V_0}\right)^{-\frac{2}{3}} - 1\right]\right\} \quad (1)$$

where P and V is the pressure and the volume at 0 GPa, respectively.

The enthalpy (H) of the Ga_8As_{32} and $Ga_{32}As_8$ clusters was also calculated, which depends on the total energy (E_{tot}), P and V of the studied system. It is defined as

$$H = E_{tot} + PV \quad (2)$$

where $P = dE_{tot}/dV$ which can be found out by the energy-volume curves. Thus, I plotted E versus P graph to see the two transition pressures (see Fig. 4) which were predicted as approximate −6.2 and −5.8 GPa are obtained as $P\bar{4}3m \rightarrow P\bar{1}$ and $P\bar{4}3m \rightarrow P\bar{4}$ for Ga_8As_{32} and $Ga_{32}As_8$ clusters.

The changes in the cell lengths and angles based on the minimization step is indicated in Fig. 5(a and b). Fig. 5(a), there is no change in the α, β and γ angles of the Ga_8As_{32} cluster at 40 GPa up to almost 40^{th} step, after this step, the α and γ angles sharply increase up to about 100^{th} step where (about 105^0) and then the angles do not change until the optimization process finish. However, the β angle decreases at the almost 100^{th} step and after 72^0, they remain stable throughout the simulation. The small changes took place in the lattice lengths A, B, and C up to about 70^{th} step. Then, A and B increase up to about 10.5 Å, as C decreases up to about 8 Å at 90^{th} step. Later, they keep steady during the simulation. For $Ga_{32}As_8$ cluster at 70 GPa given in Fig. 5(b), there is no change in the α, β and γ angles till almost 30^{th} step where the α and γ angles sharply increase up to almost 90^{th} step, and after about 94^0 decrease up to 90^0. On the other hand, β angle starts to drop at almost 80^{th} step. It increases up to 90^0 again after 85^0 and then

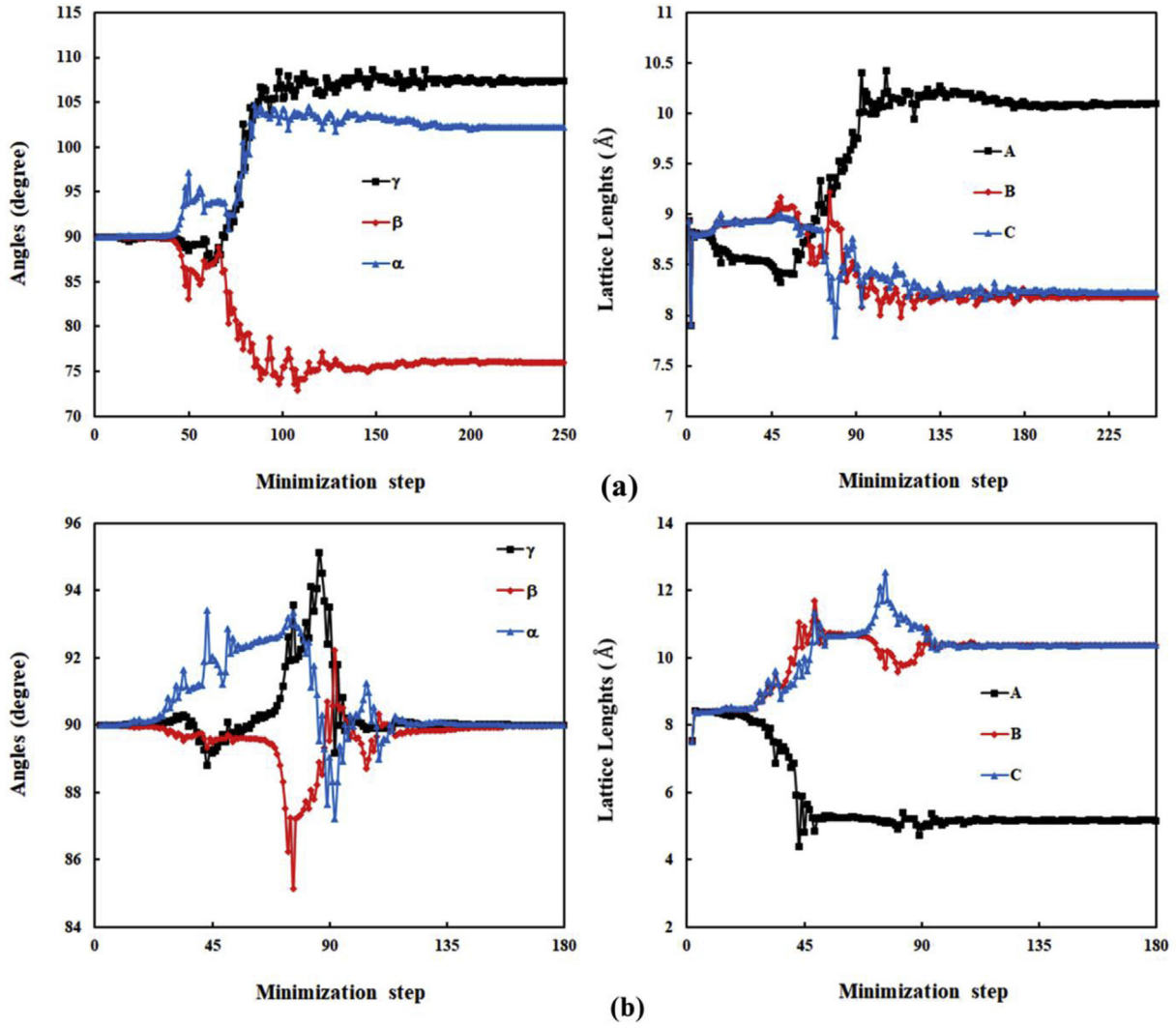

Fig. 5. The behavior of the simulation cell lengths and angles as function of minimization steps: (a) at 40 GPa and (b) at 70 GPa for (a) the Ga_8As_{32} and (b) $Ga_{32}As_8$ clusters, respectively.

they remain constant. The lattice lengths A, B and C for the $Ga_{32}As_8$ cluster are constant up to almost 30th step after this step, the B and C lengths increase while the C length decreases. The B and C lengths don't change up to 11.5 Å and then the length C start to increase up to 12.3 Å, while the B decreases up to 10 Å. After that, the lengths B and C remain constant during the minimization step. In the literature, there no information about the changes in the cell lengths and angles to compare the results. From the results mentioned above, one can conclude that the parameters highly depend on the composition and pressure.

The intermediate states occurred during the phase transforms (at 40 and 70 GPa) was also investigated in each simulation step of the Ga_8As_{32} and $Ga_{32}As_8$ clusters. From the results, the $P\overline{1}$ phase of Ga_8As_{32} cluster is composed of two intermediate states with space groups Cm at 45th step and $P1$ at 60th step. The $P\overline{4}$ phase of $Ga_{32}As_8$ cluster includes four intermediate phases with space group $P\overline{4}2m$ at 26th step, $P222$ at 39th step, $P2$ at 50th step and $P1$ at 69th step.

The formation of a stable structure for some materials is one of the major problems [33] to get high-efficiency solar cell devices. Atom distribution in crystalline structures is in general uniform and homogeneous [34]. This behavior at the nanoscale may not be conserved, especially under heat treatment [35,36]. Thus, the order parameter (R_A) is calculated to research the stable structure in a cluster by analyzing the distribution of atoms with the different types [36]. R_A is identified by the average distance of a type A atoms in accordance with the center of a cluster,

$$R_A = \frac{1}{n_A}\sum_{i=1}^{n_A} r_i \tag{3}$$

where n_A is the number A type atoms in the binary AB cluster, and r_i are the distances of the atoms to the coordinate center of the cluster. If R_A is a small value, it means that A type atoms are at the center, if R_A is a large value, it means that A type atoms are at the surface region of a cluster and if R_A is a medium value, it means a well-mixed cluster.

Fig. 6 indicates the behavior of R Ga and As atoms in accordance with pressure for the Ga_8As_{32} and $Ga_{32}As_8$ clusters. It is seen that As atoms are generally on the surface due to the lower cohesive energy of As atoms than Ga atoms (−2.99 eV) [37] and thus they move away from the inner regions of the clusters to the surface regions. Ga atoms are found to be at the center. $Ga_{32}As_8$ cluster has also larger value than that of the Ga_8As_{32}. Depending on the rise of pressure, Ga and As atoms show a tendency to the inner regions.

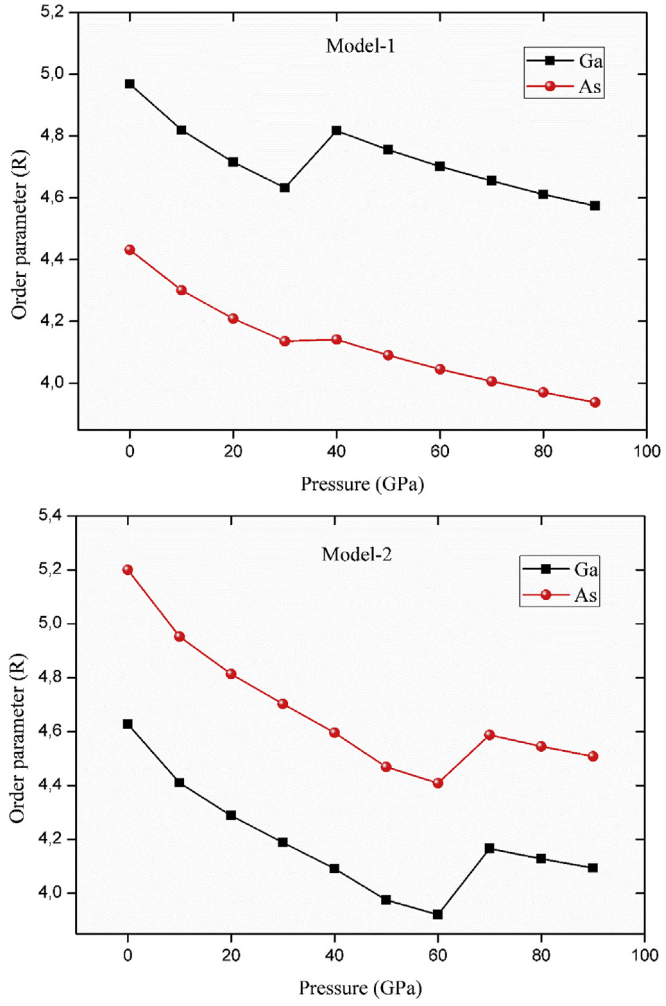

Fig. 6. The behavior of the order parameter (R) of Ga and As atoms in terms of pressure for (a) the Ga_8As_{32} and (b) $Ga_{32}As_8$ clusters.

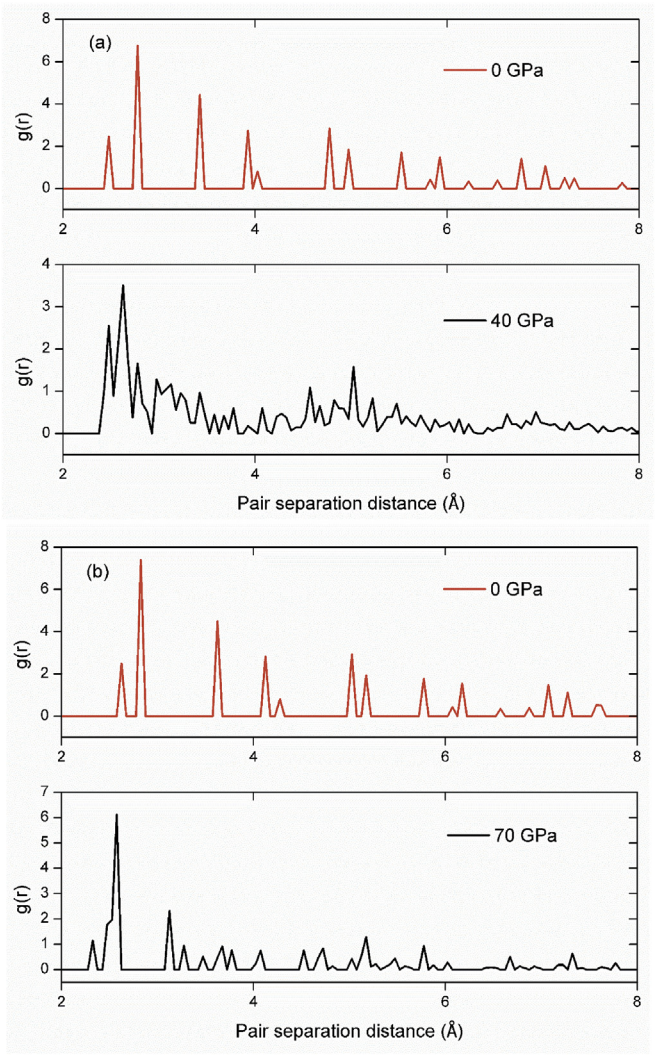

Fig. 7. Radial distribution functions (RDFs) according to the pair separation distance of (a) the Ga_8As_{32} and (b) $Ga_{32}As_8$ clusters at different pressures.

The radial distribution functions (RDFs) was analyzed for pair separation distance. Fig. 7 shows the RDF of the Ga_8As_{32} and $Ga_{32}As_8$ clusters at 40 and 70 GPa for the Ga_8As_{32} and $Ga_{32}As_8$ clusters. One can see that Ga-Ga and As-As have a narrower and higher distribution than the other pair interactions for the Ga_8As_{32} and $Ga_{32}As_8$ clusters, respectively. After the phase transition, the value of RDF decreases for all binary interactions. Moreover, the fluctuations of obvious peaks in RDF also increase with raising pressure. The peaks of the RDF for the Ga_8As_{32} at 0 GPA are sharper than that of the Ga_8As_{32} at 40 GPa and the $Ga_{32}As_8$ cluster at 0 and 70 GPa.

3.2. Electronic structure

Fig. 8 (a, b) shows the energy dependence of density of states (DOS) of the Ga_8As_{32} and $Ga_{32}As_8$ clusters at different pressures. The DOS of the Ga_8As_{32} at 0 GPa is higher than that of 40 GPa, while it is almost the same at 0 and 70 GPa for the $Ga_{32}As_8$. The higher state means the atoms accumulate inside more in the simulation cell. The HOMO, LUMO, and Fermi energies (E_f) of the Ga_8As_{32} and (b) $Ga_{32}As_8$ clusters up to 90 GPa are tabulated in Table 2. The Ga_8As_{32} has the HOMO and LUMO levels of around −3.9 eV and −2.7 eV at 0 GPa. The corresponding E_f is −3.3 eV which is located in the middle of the energy gap. This trend continues up to 90 GPa, but the HOMO, LUMO and Fermi energies almost remain constant after 60 GPa. Especially, after the transform occurs at 40 GPa, there are considerable changes in LUMO and Fermi levels (about 0.85 eV and 0.50 eV, respectively). For the $Ga_{32}As_8$, there is no significant change in HOMO, LUMO and Fermi levels as observed in the $Ga_{32}As_8$ despite the pressure increase and phase transition (see Table 2). The changes in the corresponding energy gaps based on pressure were shown in Fig. 9 (a, b). The gap energy for the Ga_8As_{32} cluster was predicted as about 1.22 eV wide, i.e., about 0.30 eV smaller than the measured band gap of bulk $Ga_{0.5}As_{0.5}$ 1.52 eV at T = 0 K [38], while the gap energy for the $Ga_{32}As_8$ is found as 0.15 eV which is due to the increase in the lattice constant by increasing the Ga concentration. An increase was observed in the gap energies up to 20 GPa for the Ga_8As_{32} and then it starts to slightly decrease up to 40 GPa where the phase transition occurs. It is interesting to note that the gap energy sharply decreases from 1.24 eV to 0.54 eV after the phase transition occurs and then it remains constant between 70 and 90 GPa. In the literature, the effect of pressure on the energy gap has been experimentally investigated up to ~20 GPa where the predicted results in this study were found to be very good. For example, a linear increase was observed up to 9 and 10 GPa without any structural phase transformations [39,40].

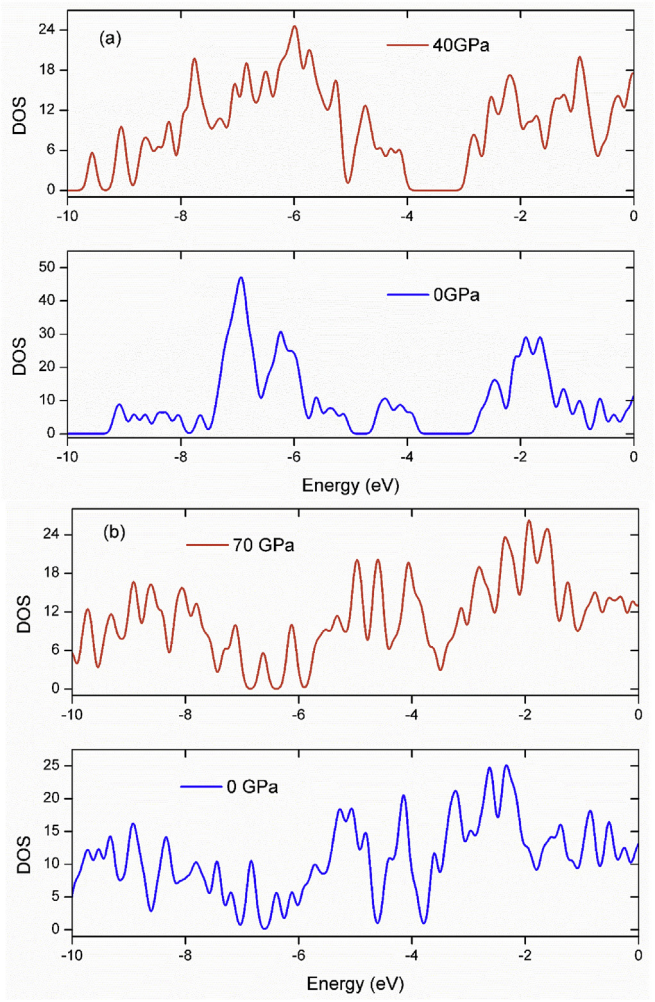

Fig. 8. The density of state of (a) the Ga_8As_{32} and (b) $Ga_{32}As_8$ clusters at different pressures.

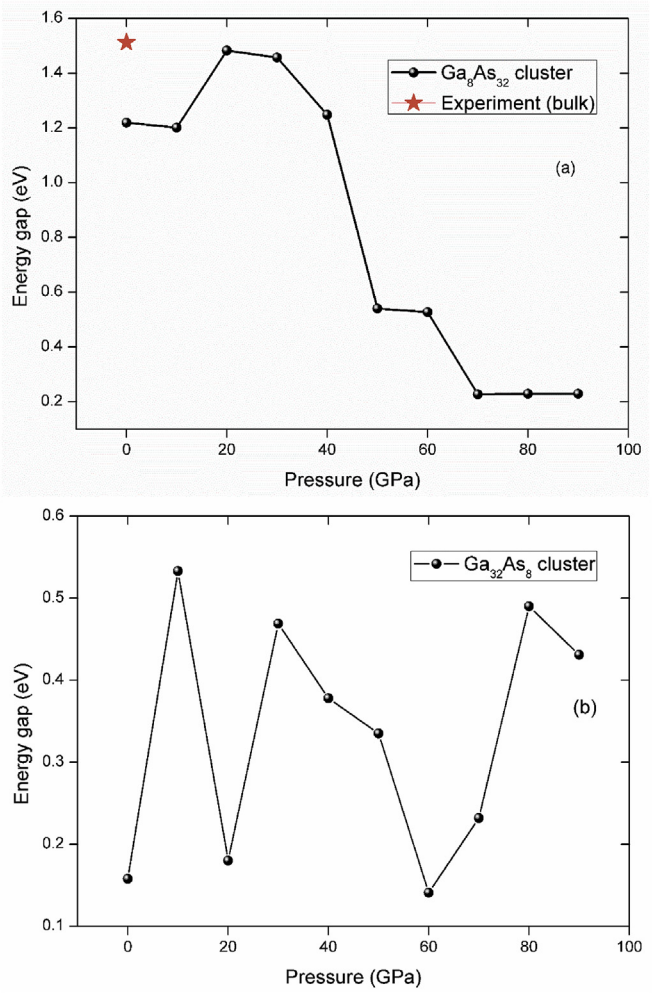

Fig. 9. The variations of the energy gap of (a) the Ga_8As_{32} and (b) $Ga_{32}As_8$ clusters at different pressures.

Table 2
The HOMO, LUMO and Fermi energies (E_f) [eV] according to pressure (GPa).

Pressure	Ga_8A_{32}			$Ga_{32}A_8$		
	HOMO	LUMO	E_f	HOMO	LUMO	E_f
0	−3.921	−2.702	−3.311	−3.607	−3.449	−3.528
10	−3.895	−2.694	−3.294	−3.777	−3.244	−3.510
20	−4.070	−2.587	−3.328	−3.680	−3.500	−3.589
30	−4.039	−2.582	−3.310	−3.698	−3.229	−3.463
40	−4.129	−2.881	−3.504	−3.741	−3.363	−3.551
50	−4.276	−3.736	−4.006	−3.651	−3.316	−3.483
60	−4.155	−3.628	−3.891	−3.686	−3.545	−3.615
70	−4.131	−3.904	−4.017	−3.614	−3.382	−3.498
80	−4.131	−3.902	−4.016	−3.701	−3.211	−3.456
90	−4.132	−3.903	−4.017	−3.675	−3.244	−3.548

In another experiment which is up to 18 GPa, the same trend was observed, but the increase of the gap energy continued with a decreasing trend after 10 GPa [41]. These results are compatible with the predictions in this study. For the $Ga_{32}As_8$, the energy gap increases up to 10 GPa like in the experiments [30–41]. After that pressure, the gap energy decreases up to 60 GPa except for 20 GPa where it suddenly drops from 0.53 eV to 0.18 eV and the increase in the pressure between 70 and 80 GPa gives rise to an increase in the gap energy, but it again decreases a little at 90 GPa. On the other hand, in the literature, there are some studies on the pressure dependence properties of GaAs, but these studies are on very low pressure (up to 18 GPa) as mentioned above when compared to this study. Thus, I compared the results obtained from this study with experimental results at 0 GPa in Fig. 9(a). Moreover, the trend of band gap is similar to experimental results [41] in the range of 0–17 GPa. In that range, band gap decreases at 16 GPa, then it increases at 17 GPa. This behavior is observed between 0 and 20 GPa in this study.

The temperature dependence of the energy gap has also been investigated for the Ga_8As_{32} and $Ga_{32}As_8$ clusters. The HOMO, LUMO, Fermi levels and energy gaps were tabulated in Table 3. The variation of the HOMO, LUMO and gap energies were given in Figs. 10 and 11, respectively. For this purpose, I used the available experimental data [42–44] to perform temperature dependence of the Ga_8As_{32} cluster. I have taken into consideration some specific temperature like in the experiment. The HOMO, LUMO and Fermi levels change in the same manner. For example, the levels increase from 55 K to 90 K, while they decrease from 273 K to 473 K. When it comes to the energy gap, it decreases from 55 K to 473 K. Comparison with experiment [42–44], the trend of the energy gap is good agreement (see Fig. 11) for the both clusters. The predicted energy gap of the Ga_8As_{32} cluster (1.29 eV) at 0 K and 0 GPa is found to be bigger than that of the $Ga_{32}As_8$ (~0.16 eV), which is due to the increase in the lattice constant by increasing the Ga concentration.

Table 3
The HOMO, LUMO and Fermi energies (E_f) [eV] according to different temperatures (K).

Temperature	Ga_8A_{32}			$Ga_{32}A_8$		
	HOMO	LUMO	E_f	HOMO	LUMO	E_f
55	−3.983	−2.601	−3.292	−3.676	−3.525	−3.600
90	−3.932	−2.576	−3.254	−3.707	−3.696	−3.613
273	−3.857	−2.560	−3.208	−3.984	−3.922	−3.625
473	−3.894	−2.675	−3.284	−4.033	−3.973	−3.498

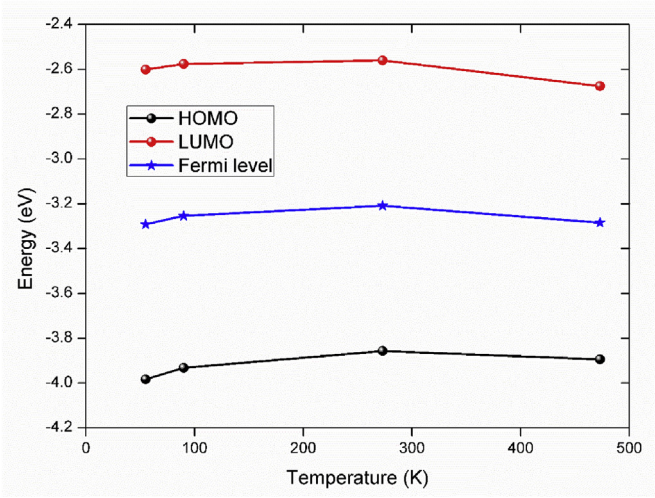

Fig. 10. The variations of the HOMO, LUMO and Fermi levels of the Ga_8As_{32} cluster at different temperatures.

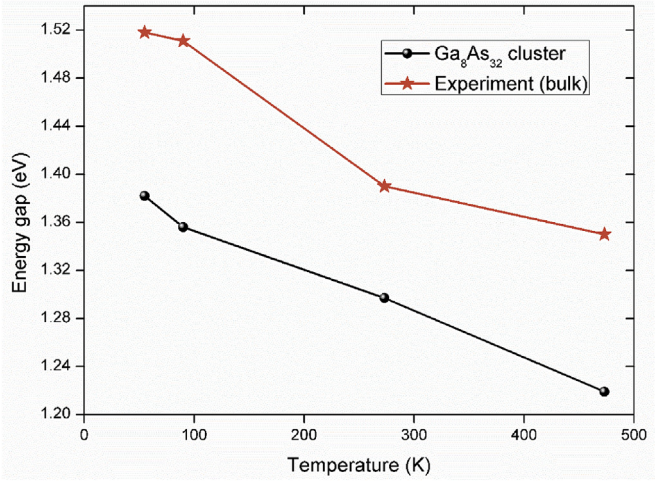

Fig. 11. The variations of the energy gap of the Ga_8As_{32} cluster at different temperatures.

The band energy of the Ga_8As_{32} cluster decreases 1.35 eV (at 55 K) to 1.21 eV (at 473 K), but that of the $Ga_{32}As_8$ cluster decreases from 0.16 eV (at 55 K) to 0.06 eV (at 473 K). It is interesting to note that the Ga_8As_{32} cluster shows still a semiconductor character at even high temperatures, while the $Ga_{32}As_8$ cluster indicates a metallic character after reaching 90 K.

The dipole moment (D_M) results from differences in electronegativity. The bigger D_M corresponds to stronger intermolecular interaction. At this viewpoint, the x, y and z components of D_M under pressure and temperature are given in Tables 4 and 5. The

Table 4
The dipole moments (D_M, Debye) in x, y and z directions under high pressure (GPa).

Pressure	Ga_8A_{32}			$Ga_{32}A_8$		
	D_x	D_y	D_z	D_x	D_y	D_z
0	4.5091	−0.6283	0.9861	−1.2956	−0.0103	−1.0411
10	1.5910	−0.8492	4.3219	6.9101	2.3131	7.2954
20	0.4090	3.7170	1.8464	−1.4324	−0.1130	−1.4672
30	1.2167	2.9791	0.9214	−1.5450	1.5992	−0.2633
40	2.0856	−1.4296	−1.9047	0.2406	−0.7780	−1.8119
50	−4.6657	−2.2048	2.4468	5.3392	10.137	0.9345
60	−5.4124	−2.3404	3.7149	0.9345	1.6568	−2.5632
70	−4.9629	−4.2420	2.2715	1.8492	−2.4459	−0.0160
80	−5.0009	−4.1942	2.4159	−1.3801	0.3939	−2.8196
90	4.9970	−4.2078	2.4018	0.7215	0.9589	0.7187

Table 5
The dipole moments (D_M, Debye) in x, y and z directions at different temperature (K).

Temperature	Ga_8A_{32}			$Ga_{32}A_8$		
	D_x	D_y	D_z	D_x	D_y	D_z
55	0.4260	1.4141	3.2867	8.3925	2.8776	5.6963
90	1.3454	3.3582	4.0475	5.6213	1.6081	6.6555
273	1.2750	0.3412	2.9070	5.3709	1.5363	6.5113
473	3.8413	1.8717	4.2895	−1.4856	1.8785	−0.4152

component of D_M along the x-axis (−5.4124 Debye) at 60 GPa for the Ga_8As_{32} cluster gives rise to large negative charge separation in the x-direction. The biggest component of D_M for the Ga_8As_{32} cluster is found to be along the y-axis (10.137 Debye) at 60 GPa which means large charge separation in the y-direction. The bigger value of D_M for the Ga_8As_{32} than the Ga_8As_{32} indicates that the Ga_8As_{32} cluster has stronger intermolecular interaction. These values are comparable with the gap energies because the lowest gap energy of the Ga_8As_{32} cluster means that electrons easily transfer from HOMO to LUMO. In this regard, there is a highly relevant correlation between D_M and the energy gap of the Ga_8As_{32} and the Ga_8As_{32} clusters. Thus, I can conclude that the large D_M has small the energy gap.

4. Conclusions

The tunable electronic structure and structural transition of GaAs clusters with different compositions at high pressure and temperature were performed by quantum chemical calculations for the first time. The phase transformations from the zinc blende to triclinic and tetragonal phases have been determined. The structural properties at transition pressures were analyzed where it was found two and four intermediate phases. The As-rich clusters are generally more stable than that of the Ga-rich. The electronic structure such as HOMO, LUMO dipole moment and energy gap may be tuned based on pressure and temperature. The analysis of energy gap implies that the Ga_8As_{32} cluster shows still a semiconductor character at even high temperatures, while the $Ga_{32}As_8$ cluster indicates a metallic character after reaching 90 K. The large dipole moment has a small the energy gap. The energy band of the clusters is also compatible with available experimental findings. Obtained results herein show that the GaAs clusters with different compositions contain very interesting results under high pressure and temperature. This may provide significant contributions to advances in the applications of detectors, transistors, solar cells and optoelectronic devices based on the GaAs material.

References

[1] M.S. Al-Ghamdi, A. Sayari, L. Sfaxi, J. Alloys Compd. 685 (2016) 202–208.

[2] P. Pluengphon, T. Bovornratanaraks, S. Vannarat, U. Pinsook, Solid State Commun. 195 (2014) 26–30.
[3] A. Smida, F. Laatar, M. Hassen, H. Ezzaouia, J. Lumin. 176 (2016) 118–123.
[4] H. Saghrouni, S. Jomni, A. Cherif, W. Belgacem, L. Beji, J. Alloys Compd. 676 (2016) 127–134.
[5] A. Salhi, S. Alshaibani, Y. Alaskar, A. Albadri, A. Alyamani, J. Alloys Compd. 771 (2019) 382–386.
[6] F. Schlaepfer, M. Lucchini, S.A. Sato, M. Volkov, L. Kasmi, N. Hartmann, A. Rubio, L. Gallmann, U. Keller, Nat. Phys. 14 (2018) 560–564.
[7] S. Moon, K. Kim, Y. Kim, J. Heo, J. Lee, Sci. Rep. 6 (2016), 30107-1- 30107-6.
[8] Q. Li, K. Shen, R. Yang, Y. Zhao, S. Lu, R. Wang, J. Dong, D. Wang, Sol. Energy 157 (2017) 216–226.
[9] L. Brus, J. Phys. Chem. 90 (1986) 2555–2560.
[10] A. Graf, D. Sonnenberg, V. Paulava, A. Schliwa, Ch. Heyn, W. Hansen, Phys. Rev. B 89 (2014), 115314-1-115314-6.
[11] G. Sallen, S. Kunz, T. Amand, L. Bouet, T. Kuroda, T. Mano, D. Paget, O. Krebs, X. Marie, K. Sakoda, B. Urbaszek, Nat. Commun. 5 (2014), 3268-1-3268-7.
[12] Z. Syum, H. Woldeghebriel, J. Clust. Sci. 27 (2016) 551–561.
[13] R. Moussa, A. Abdiche, B. Abbar, M. Guemou, R. Riane, G. Murtaza, S.B. Omran, R. Khenata, F. Soyalp, J. Electron. Mater. 44 (2015) 4684–4699.
[14] S.C. Yu, I.L. Spain, E.F. Skelton, Solid State Commun. 25 (1978) 49–52.
[15] M.A. Baublitz, A.L. Ruoff, J. Appl. Phys. 53 (1982) 6179–6185.
[16] S.B. Zhang, M.L. Cohen, Phys. Rev. B 39 (1989) 1450–1452.
[17] S. Ono, T. Kikegawa, J. Phys. Chem. Solids 113 (2018) 1–4.
[18] M.I. McMahon, R.J. Nelmes, Phys. Status Solidi B 198 (1996) 389–402.
[19] A. Mujica, R.J. Needs, J. Phys. Condens. Matter 8 (1996) L237–L243.
[20] P. Ordejon, E. Artacho, J.M. Soler, Phys. Rev. B 53 (1996) 441–444. R10.
[21] J.P. Perdew, K. Burke, M. Ernzerhof, Phys. Rev. Lett. 77 (1996) 3865–3868.
[22] H.J. Monkhorst, J.D. Pack, Phys. Rev. B 13 (1976) 5188–5192.
[23] R. Hundt, J.C. Schön, A. Hannemann, M.J. Jansen, Appl. Crystallogr. 32 (1999) 413–416.
[24] A. Hannemann, R. Hundt, J.C. Schön, M.J. Jansen, Appl. Crystallogr. 31 (1998) 922–928.
[25] B. Aradi, B. Hourahine, T. Frauenheim, J. Phys. Chem. A 111 (2007) 5678–5684.
[26] Z. Hajnal, Th. Frauenheim, C. González, J. Ortega, R. Pérez, F. Flores, Appl. Surf. Sci. 212–213 (2003) 861–865.
[27] Z. Hajnal, R. Scholz, S. Sanna, Th. Frauenheim, Appl. Surf. Sci. 234 (2004) 173–177.
[28] K.H. Hellwege, O. Madelung, Landolt-Bornstein, Semiconductors: Physics of Group IV Elements and III–V Alloys, New Series, Group III, 1982, p. 17.
[29] M. Othman, E. Kasap, N. Korozlu, J. Alloys Compd. 496 (2010) 226–233.
[30] G.W. Lemire, G.A. Bishea, S.A. Heidecke, M.D. Morse, J. Chem. Phys. 92 (1990) 121–132.
[31] F. Birch, Phys. Rev. 71 (1947) 809–824.
[32] F.D. Murnaghan, Proc. Natl. Acad. Sci. U.S.A. 30 (1944) 244–247.
[33] T.C. Yu, R.F. Brebrick, J. Phase Equilib. 13 (1992) 476–496.
[34] C. Lu, Y. Cheng, Q. Pan, X. Tao, B. Yang, G. Ye, Sci. Rep. 6 (2016), 19870-19871-19870-7.
[35] M. Kurban, O.B. Malcıoğlu, Ş. Erkoç, Chem. Phys. 464 (2016) 40–45.
[36] M. Kurban, Ş. Erkoç, Physica E 88 (2017) 243–251.
[37] D.A. Murdick, X.W. Zhou, H.N.G. Wadley, Phys. Rev. B 73 (2006), 045206-1-045206-20.
[38] C. Data from Kittel, Introduction to Solid State Physics, sixth ed., John Wiley, New York, 1986, p. 185.
[39] W.P. Zurawsky, J.E. Littman, H.G. Drickamer, J. Appl. Phys. 54 (1983) 3216–3219.
[40] A.R. Goñi, A. Cantarero, Svassen K.M. Cardona, High Press. Res. 3 (1990) 81–83.
[41] B. Welber, M. Cardona, C.K. Kim, S. Rodriguez, Phys. Rev. B 12 (1975) 5729–5738.
[42] M.B. Panish, H.C. Casey, J. Appl. Phys. 40 (1969) 163–167.
[43] F.J. Blatt, Modern Physics, McGraw-Hill, 1992.
[44] M.D. Sturge, Phys. Rev. 127 (1963) 768–773.